# Hierarchical porosity in self-assemhled polymers

Valkama, Sami; Nykanen, Antti; Kosonen, Harri; Ramani, Ramasubbu; Tuomisto, Filip; Engelhardt, Peter; ten Brinke, Gerrit; Ikkala, Olli; Ruokolainen, Janne; Nykänen, Antti

*Published in:*
Advanced Functional Materials

*DOI:*
10.1002/adfm.200600604

ADVANCED FUNCTIONAL MATERIALS

FULL PAPER

DOI: 10.1002/adfm.200600604

# Hierarchical Porosity in Self-Assembled Polymers: Post-Modification of Block Copolymer–Phenolic Resin Complexes by Pyrolysis Allows the Control of Micro- and Mesoporosity**

By *Sami Valkama*, *Antti Nykänen*, *Harri Kosonen*, *Ramasubbu Ramani*, *Filip Tuomisto*, *Peter Engelhardt*, *Gerrit ten Brinke*, *Olli Ikkala*,* and *Janne Ruokolainen**

It is shown that self-assembled hierarchical porosity in organic polymers can be obtained in a facile manner based on pyrolyzed block-copolymer–phenolic resin nanocomposites and that a given starting composition can be post-modified in a wide range from monomodal mesoporous materials to hierarchical micro-mesoporous materials with a high density of pores and large surface area per volume unit (up to 500–600 $m^2 g^{-1}$). For that purpose, self-assembled cured composites are used where phenolic resin is templated by a diblock copolymer poly(4-vinylpyridine)-*block*-polystyrene (P4VP-*b*-PS). Mild pyrolysis conditions lead only to monomodal mesoscale porosity, as essentially only the PS block is removed (length scale of tens of nanometers), whereas during more severe conditions under prolonged isothermal pyrolysis at 420 °C the P4VP chains within the phenolic matrix are also removed, leading to additional microporosity (sub-nanometer length scale). The porosity is analyzed using transmission electron microscopy (TEM), small-angle X-ray scattering, electron microscopy tomography (3D-TEM), positron annihilation lifetime spectroscopy (PALS), and surface-area Brunauer–Emmett–Teller (BET) measurements. Furthermore, the relative amount of micro- and mesopores can be tuned in situ by post modification. As controlled pyrolysis leaves phenolic hydroxyl groups at the pore walls and the thermoset resin-based materials can be easily molded into a desired shape, it is expected that such materials could be useful for sensors, separation materials, filters, and templates for catalysis.

[*] Prof. O. Ikkala, Dr. J. Ruokolainen
Optics and Molecular Materials and Center for New Materials
Helsinki University of Technology
P.O. Box 2200, 02015 TKK, Espoo (Finland)
E-mail: Olli.Ikkala@tkk.fi; Janne.Ruokolainen@tkk.fi
S. Valkama, A. Nykänen, Dr. H. Kosonen, Dr. R. Ramani
Optics and Molecular Materials and Center for New Materials
Helsinki University of Technology
P.O. Box 2200, 02015 TKK, Espoo (Finland)
Dr. F. Tuomisto
Laboratory of Physics, Helsinki University of Technology
P.O. Box 1100, 02015 TKK, Espoo (Finland)
Dr. P. Engelhardt
Laboratory of Computational Engineering
Helsinki University of Technology
P.O. Box 9203, 02015 TKK (Finland)
Dr. P. Engelhardt
Department of Pathology and Virology
Haartman Institute
P.O. Box 21, 00014, University of Helsinki (Finland)
Prof. G. ten Brinke
Materials Science Center, University of Groningen
Nijenborgh 4, 9747 AG Groningen (The Netherlands)

[**] Ari Laiho, Kati Vilonen, Simo Kilpeläinen, and Jani Päiväsaari from Helsinki University of Technology are acknowledged for experimental assistance. Ville Lilja from Laboratory of Computational Engineering, Helsinki University of Technology is acknowledged for experimental assistance and discussions related to Transmission Electron Tomography. Beamtime on the BM26B (DUBBLE) has kindly been made available by The Netherlands Organization for Scientific Research (NWO) and we acknowledge Dr. Wim Bras and Florian Meneau for experimental assistance and discussions. This work was carried out in the Centre of Excellence of Finnish Academy ("Bio- and Nanopolymers Research Group", 77317) and supported by the European Commission-project COMPOSE project no. NMP3-CT-2003-505633.

## 1. Introduction

Nature provides several examples where hierarchical porosity is essential for functionality and it facilitates efficient transport of fluids or gases in plants, wood, lungs, and bones. Compared to poorly defined porosity within materials consisting of large pore size distribution and materials consisting of monomodal porosity of narrow pore size distribution at one length scale, well-controlled hierarchical porosity can lead to enhanced transport over larger distances based on continuous macroporous channels (sizes >50 nm), combined with micropores (<2 nm) and mesopores (2–50 nm), which promote high surface area, activity, and selectivity.[1] Also, in materials science, hierarchically porous materials have recently been extensively investigated for different applications such as catalysis, biomaterial engineering, separation, filters, electronics, and optoelectronics.[2–5] In this area, hierarchical porosity has been investigated using inorganic matter such as zeolites, sol–gel materials, various silica templates, and monoliths, where self-assembly has also been used to allow highly controlled structures; for an extensive list of the literature see the reviews that have been published.[4,6–9] The length scale of the porosity is typically controlled by selecting different starting-material compositions and molecular weights for the templates. In synthetic polymers, well-defined hierarchical porosity facilitated by self-assembly is less studied,[10] even if there is extensive literature for monomodal polymeric porosity.

Using inorganic matter, several concepts to prepare hierarchical bi- or trimodal porous materials have been reported previously, including, micro-macroporous,[11] micro-mesoporous,[12] meso-macroporous,[4,13–16] bimodal mesoporous,[17,18] bimodal mesoporous-macroporous,[19] and micro-meso-macroporous materials.[20,21] Among the various concepts, the template-assisted approach provides a facile way for well-defined structures at different length scales, for a wide range of pore sizes, and for various chemical functionalities.[5,16,22–24] Examples of suitable structure-directing agents include, surfactants or block copolymers,[25–31] colloids,[32,33] emulsions,[34] polymer gels,[35] vesicles,[36] foams,[13,37] solid particles, and bacteria.[38] By combining different structure-directing agents, the structures can be controlled hierarchically at different independent length scales.

Block copolymers provide feasible materials for templates, as they self-assemble into various structures such as spherical, cylindrical, lamellar, gyroid, and more complicated phases.[39] Previously it has been shown that upon mixing uncured phenolic resins and block copolymers consisting of a block that forms strong enough hydrogen bonds with the phenolic hydroxyls, the phenolic resin can be cured, still preserving the self-assembly without macroscopic phase separation.[30,31,40,41] In addition, the structure-directing block-copolymer template can be removed afterwards by controlled pyrolysis leading to a monomodal mesoporous material with a well-defined length scale.[29,30] In this work the pyrolysis conditions were observed that allow even hierarchical porosity as a facile post-modification step in phenolic resin–poly(4-vinylpyridine)-*block*-polystyrene (P4VP-*b*-PS) complexes. Mild pyrolysis conditions lead only to monomodal mesoscale porosity, as essentially only the PS block is removed, whereas during more severe conditions under prolonged isothermal pyrolysis at 420 °C the P4VP chains within the phenolic matrix are also removed leading to additional microporosity. Owing to the bimodal micro-mesoporous structure, these materials have large surface areas (500–600 $m^2 g^{-1}$). In addition, as controlled pyrolysis leaves phenolic hydroxyl groups at the pore walls and the materials can be practically molded into any desired shape, not existing only as powders, their range of applications is increased significantly.[42,43]

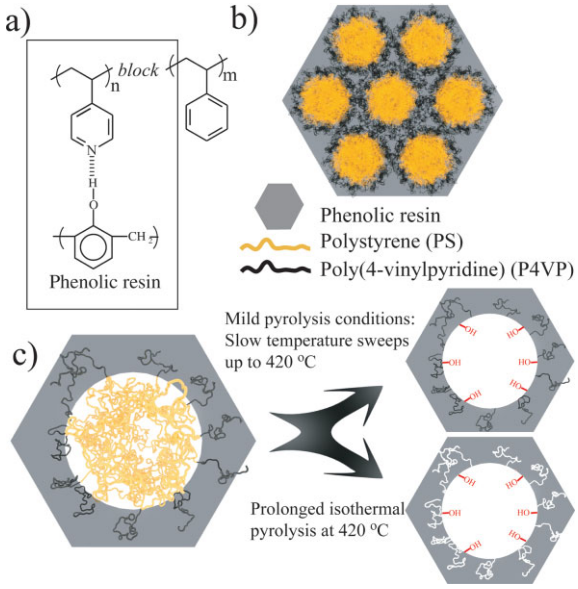


**Figure 1.** a) Phenolic resin, P4VP-*b*-PS and schematics of their mutual hydrogen bonding. b) As a result of hydrogen bonding, the phenolic resin and P4VP are confined within the same self-assembled domains as they microphase-separate from the nonpolar PS domains. Crosslinking at elevated temperatures "locks" the structure. c) By selecting different pyrolysis conditions, the relative fraction of meso- and microporosity can be tuned. Mild pyrolysis conditions lead to mesoporous material, as essentially only the PS block is removed. Hierarchical porous materials can be obtained with prolonged isothermal pyrolysis at 420 °C, when both blocks of P4VP-*b*-PS are removed. These porous materials have a narrow distribution of pore sizes, high surface area per volume unit, and hydroxyl groups at the matrix and pore walls.

## 2. Results and Discussion

A P4VP-*b*-PS block copolymer (number-average molecular weight: $M_{n,P4VP} = 5600\ g\,mol^{-1}$, $M_{n,PS} = 40\,000\ g\,mol^{-1}$, and polydispersity index 1.09) was used to prepare mixtures with the phenolic resin (Vulkadur RB, Bayer) and curing agent hexamethylenetetramine (HMTA); see Figure 1a for the schematic structures. Owing to the hydrogen bonding between the pyridines and phenolic resin,[40] self-assembled structures consisting of periodic PS and P4VP–phenolic resin domains are formed (Fig. 1b). Based on our previous studies[29] the relative weight fraction of PS in the composition is fixed to 40 %, which leads to self-assembled cylindrical PS domains. The phenolic resin domains including P4VP blocks were thermally cured at 100–190 °C. We aimed to explore if pyrolysis conditions could be identified that would allow distinct and controlled removal of PS from the self-assembled cylindrical domains and, importantly, removal of the P4VP chains from the P4VP–phenolic resin domains without excessive degradation of the phenolic resin (see Fig. 1c). A couple of considerations are relevant when selecting the pyrolysis conditions. First, slow heating at a rate of $1\ °C\,min^{-1}$ was selected to minimize the structural deformations. Second, previous experience[29] suggested that ca. 420 °C could not be exceeded to limit the removal of the phenolic-resin phase. Therefore, an isothermal treatment at 420 °C was used to allow hierarchical porosity. Table 1 lists the prepared samples, the pyrolysis conditions, as well as the obtained surface areas.

The structures of the cured and pyrolyzed phenolic resin–P4VP-*b*-PS complexes (40 wt % PS) were first analyzed using transmission electron microscopy (TEM) and small-angle X-ray scattering (SAXS). Figure 2 displays the TEM images after different pyrolysis conditions. Before pyrolysis a cylindrical structure was obtained with a periodicity of ca. 55 nm and the diameter of the PS cylinders was ca. 30 nm (Fig. 2a). Pyrolysis through slowly heating up to 360 °C suggests that part of the PS cylinders is emptied, but the degradation is still incomplete (Fig. 2b). However, upon slowly heating up to $T = 420\ °C$ well-defined cylindrical pores are observed (Fig. 2c), suggesting that PS has been essentially removed. Figure 2d and e

ADVANCED FUNCTIONAL MATERIALS



**Table 1.** The pyrolysis conditions for self-assembled hierarchically porous samples and the measured surface areas. The pyrolysis is performed in air at a temperature sweep of 1 °C min–1 and all samples are cured with HMTA. The PS weight fraction is 40 % in phenolic resin–P4VP-*b*-PS complexes.

| Sample | Pyrolysis conditions | | Total surface area | Mesoporous surface area | Microporous surface area |
|---|---|---|---|---|---|
| | Final temperature [°C] | Isothermal treatment | [$m^2$ $g^{-1}$] | [$m^2$ $g^{-1}$] | [$m^2$ $g^{-1}$] |
| phenolic resin | – | – | < 5 | – | – |
| phenolic resin | – | 120 min at 420 °C | < 5 | – | – |
| phenolic resin–P4VP–*b*–PS | 330 | – | < 5 | – | – |
| phenolic resin–P4VP–*b*–PS | 360 | – | < 5 | – | – |
| phenolic resin–P4VP–*b*–PS | 390 | – | 24 | 22 | 2 |
| phenolic resin–P4VP–*b*–PS | 420 | 0 min at 420 °C | 40 | 25 | 15 |
| phenolic resin–P4VP–*b*–PS | 420 | 15 min at 420 °C | 260 | 95 | 165 |
| phenolic resin–P4VP–*b*–PS | 420 | 30 min at 420 °C | 361 | 105 | 256 |
| phenolic resin–P4VP–*b*–PS | 420 | 60 min at 420 °C | 457 | 101 | 356 |
| phenolic resin–P4VP–*b*–PS | 420 | 120 min at 420 °C | 557 | 66 | 491 |

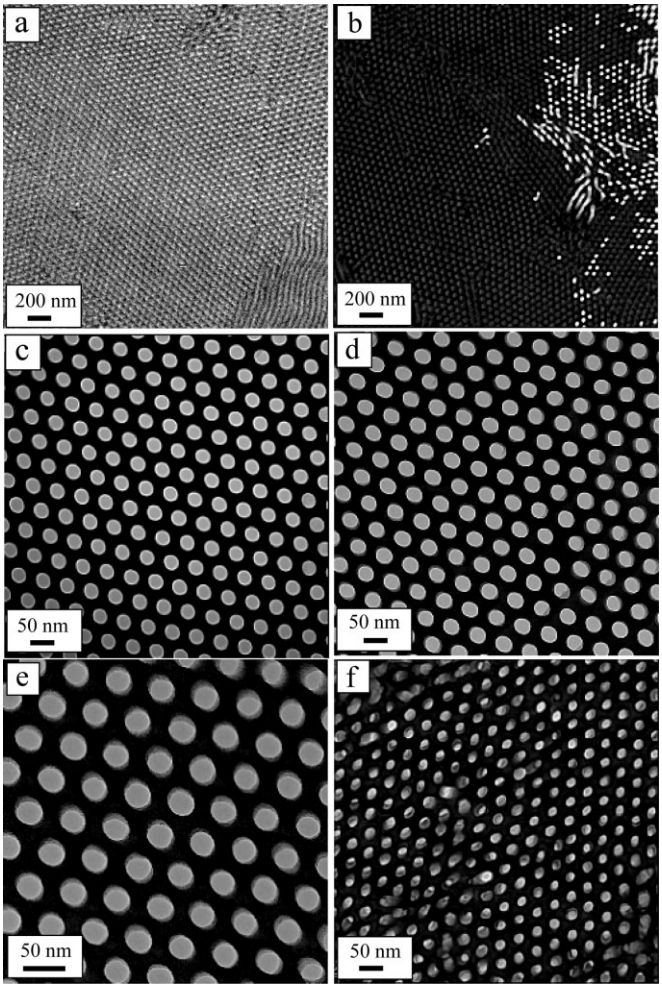


**Figure 2.** TEM images of the cured and pyrolyzed phenolic resin–P4VP-*b*-PS samples after different pyrolysis conditions representing the progress of pyrolysis. The PS weight fraction is 40 % in all cases. a) Before pyrolysis, a cylindrical PS structure with a periodicity of ca. 55 nm is observed. b) An incomplete degradation of PS is observed upon slowly heating to 360 °C (1 °C $min^{-1}$). Well-defined mesoscale cylindrical pores due to PS removal are observed for samples swept (1 °C $min^{-1}$) to 420 °C and after a subsequent isothermal treatment at 420 °C for: c) 0 min, d) 30 min, e) 60 min; and f) 120 min. In the last case, a partial collapse of the pores is observed.

shows TEM images of samples slowly heated to 420 °C and additionally isothermally treated at 420 °C for 30 and 60 min, respectively, showing essentially similar structures as that shown in Figure 2c, that is, well-defined cylindrical mesopores in the phenolic matrix. A 3D electron microscopy tomogram (see Fig. 6b) shows even more clearly the emptied cylinders. Further pyrolysis for 120 min at 420 °C leads to a slight collapse of the cylindrical pores (Fig. 2f). In conclusion, the TEM images of Figure 2 show that the self-assembled cylindrical mesoscale PS domains can be essentially emptied by the pyrolysis conditions used. However, no conclusions can be drawn from there for the P4VP chains following the pyrolysis. Note that no staining is needed in TEM for the contrast. Upon pyrolysis the electron-density contrast between the domains is increased as the block-copolymer template is removed.

Figure 3 represents SAXS curves for cured phenolic resin–P4VP-*b*-PS with 40 wt % PS prior to pyrolysis and following different pyrolysis conditions as well as for the cured pure phenolic resin and pure P4VP-*b*-PS. The pure phenolic resin shows no intensity maximum in the measured $q$ range and pure P4VP-*b*-PS has a broad reflection at $q^* = 0.031$ Å$^{-1}$. TEM, however, showed a spherical structure for the pure P4VP-*b*-PS (data not shown). For phenolic resin–P4VP-*b*-PS complexes the intensity maximum appears before pyrolysis at ca. $q^* = 0.011$ Å$^{-1}$ (corresponding to the long period of $L_p = 57$ nm) and higher-order reflection at $\sqrt{3}q^*$, $\sqrt{2}q^*$, and $\sqrt{7}q^*$ are observed, characteristic for a cylindrical structure (see Fig. 3). In addition, a broad combination peak assigned to $\sqrt{12}q^*$ and $\sqrt{13}q^*$, as well as another combination peak were observed. Upon pyrolysis the intensity pattern essentially remains. The intensity of the first reflection peak is increased upon pyrolysis, which is explained by the increased electron-density difference between the self-assembled domains. This is expected as the TEM image of Figure 2 shows that PS will be essentially removed from the cylindrical domains. For the highest degree of pyrolysis (sweep to 420 °C using 1 °C $min^{-1}$ followed by isothermal treatment for 120 min at 420 °C) the first intensity maximum and its higher-order reflections are shifted to slightly higher $q$ values ($q^* = 0.013$ Å$^{-1}$ corresponding to $L_p = 48$ nm). This agrees with the partial collapse of the cylin-

  

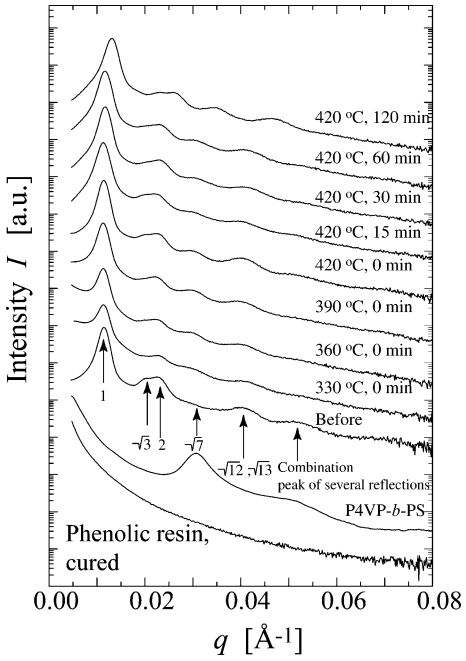


**Figure 3.** SAXS intensity patterns for the cured phenolic resin–P4VP-*b*-PS complexes before pyrolysis and after different pyrolysis treatments in air, as well as for the pure cured phenolic resin and P4VP-*b*-PS. The intensity has been Lorentz-corrected for the cylindrical structures by multiplying by the magnitude of the scattering vector *q*. The labels indicate the final temperatures after slow temperature sweeps (1 °C min$^{-1}$) and the length of the subsequent isothermal treatment. The PS weight fraction is 40 % in phenolic resin–P4VP-*b*-PS complexes.

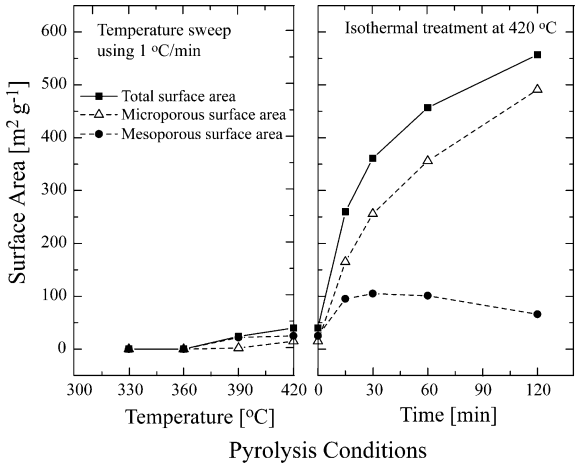


**Figure 4.** The BET surface area as a function of pyrolysis conditions for the cured and pyrolyzed phenolic resin–P4VP-*b*-PS samples after different pyrolysis conditions. The PS weight fraction is 40 % in all cases. The *x*-axis has been divided into two parts: the left side describes the pyrolysis temperature (°C) and right side the time (min) of the isothermal pyrolysis at $T = 420$ °C.

drical pores at prolonged isothermal pyrolysis, which is also suggested in the TEM images (see Fig. 2).

The previous data show that the mesoscale cylindrical domains can be emptied from the PS matter using pyrolysis. The first evidence that, in particular, the isothermal treatment is relevant to additionally remove the P4VP chains from the phenolic resin–P4VP domains comes from surface-area measurements, (see Fig. 4). The total surface areas of the samples were evaluated using the Brunauer–Emmett–Teller (BET) method and the surface area of meso- and macropores using T-plot analysis. The surface area of micropores is obtained by subtracting the surface area of meso- and macropores from the total surface area. All surface areas are summarized in Table 1 and plotted as a function of the pyrolysis conditions in Figure 4. The surface areas for pure cured phenolic resin and cured phenolic resin–P4VP-*b*-PS complexes before pyrolysis were below the resolution of the measurement system ($< 5$ m$^2$ g$^{-1}$). This was also the case for cured phenolic resin–P4VP-*b*-PS by slowly sweeping the temperature up to 330 and 360 °C. For samples pyrolyzed at 390 and 420 °C the surface areas remain relatively small and result mainly from the mesoscale porosity due to removal of the PS domain (24 m$^2$ g$^{-1}$ and 40 m$^2$ g$^{-1}$ for samples pyrolyzed at 390 and 420 °C, respectively). An additional isothermal treatment at 420 °C leads to a drastic change: the surface area resulting from the mesopores levels off after ca. 15 min of isothermal pyrolysis at $T = 420$ °C to ca. 100 m$^2$ g$^{-1}$. Note that the surface area resulting from the mesopores is slightly lower for the sample pyrolyzed at 420 °C for 120 min (66 m$^2$ g$^{-1}$), as the cylindrical pores are partially collapsed, which was observed also from TEM and SAXS results and is also evident in positron annihilation lifetime spectroscopy (PALS) measurements (see later). During the isothermal pyrolysis at 420 °C the P4VP chains within the phenolic resin matrix are also removed leading to additional microporosity, that is, hierarchical micro-mesoporous materials. The surface area owing to the micropores is drastically increased due to 120 min of isothermal pyrolysis up to ca. 500 m$^2$ g$^{-1}$, suggesting that a substantial amount of P4VP is removed from the phenolic matrix during pyrolysis, which is in agreement with our PALS results.

PALS was also used to characterize the microporosity within the phenolic matrix. PALS is a powerful in situ probe for characterization of porous materials and is applicable to sizes from sub-nanometer to nanometer scale.[44–46] In this method, the obtained ortho-positronium (o-Ps) pick-off annihilation lifetime ($\tau_3$) is directly related to the mean free-volume (micropore) size, and its intensity ($I_3$) is often interpreted to reflect the micropore volume density (see Experimental for more information about PALS).[47,48] Figure 5a and b shows the plot of $\tau_3$ and $I_3$ as a function of pyrolysis conditions. During the initial stages of pyrolysis, the $\tau_3$ value remains almost constant upon slowly heating up to 390 °C, whereas $I_3$ decreases drastically from 10 to 3.9 %. This can be explained as being due to the preferential localization of o-Ps in the mesopores formed by degradation of the PS domain (diameter ca. 30 nm) rather than in the free volume holes in the phenolic resin–P4VP-*b*-PS matrix. The existence of a lifetime component pertaining to PS mesopores was not evident in the present measurement as the gain of the spectrometer was kept constant at 0.0256 ns/channel and was aimed to characterize the size of the small P4VP

ADVANCED FUNCTIONAL MATERIALS



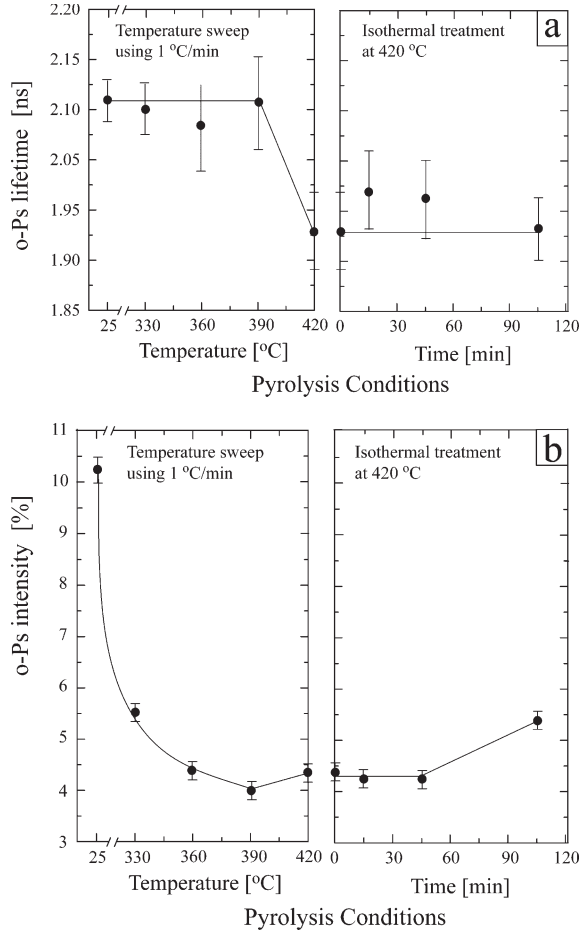


**Figure 5.** a) o-Ps lifetime ($\tau_3$) and b) o-Ps intensity ($I_3$) as a function of pyrolysis conditions. The *x*-axis has been divided into two parts: The left side describes the pyrolysis temperature (°C) and the right side the time (min) of the isothermal pyrolysis at $T = 420$ °C. Note that the sample before pyrolysis has been separated with a break in the *x*-axis.

micropores.[49–51] When the sample was slowly heated up to 420 °C, the $\tau_3$ value suddenly fell by 0.175 ns and remained almost unchanged thereafter. However, the o-Ps intensity showed a small increase at 420 °C and remained constant on the subsequent isothermal pyrolysis at 420 °C for up to 45 min. This drastic change of the o-Ps lifetime is attributed to the formation of small-sized micropores in the phenolic matrix due to the degradation of the P4VP chains, in agreement with the BET results obtained. However, no correlation could be obtained in terms of pore number ($I_3$ value) with the BET results, maybe due to the preferential localization of o-Ps in the mesopores of PS, as stated above.[52] At the final stage of isothermal pyrolysis at 420 °C, as some of the mesopores are collapsed (see Figs. 2 and 3), more o-Ps seems to form in micropores (mainly) and hence a slight raise in the $I_3$ value is observed. However, a more detailed PALS study is in progress to take into account the influence of mesopores and functional groups present at the pore walls on the characterization of micropore size and its distribution.

The mean radius of the free-volume holes can be roughly estimated by means of a simple quantum-mechanical model,[53–55] where the o-Ps in a free-volume hole is approximated to a particle in an infinite spherical potential well of radius $R_o$. The o-Ps lifetime ($\tau_3$) localized in a free-volume hole is related to its hole (assumed spherical) radius ($R$) as

$$\tau_3 = 0.5\,[1 - (R/R_o) + (1/2\,\pi)\sin(2\pi R/R_o)]^{-1}\ \text{ns} \quad (1)$$

where $R_o = R + \Delta R$ (with $\Delta R = 0.166$ nm) is an empirical parameter related to the thickness of a homogeneous electron layer surrounding the free-volume hole where o-Ps annihilates.[55] The $\tau_3$ value at each pyrolysis level was used to obtain the average pore radius using Equation 1. As the P4VP micropores are produced at 420 °C, the average pore radius below and above this temperature was found to be 0.295 and 0.282 nm, respectively. This resulted in an average micropore radius of $r = 0.27 \pm 0.01$ nm.

A final effort was made to visualize the micropores using 3D transmission electron tomography (3D-TEM). This clearly illustrates the mesoporous cylindrical structure where the PS part was removed by pyrolysis (see Fig. 6). However, more importantly, visualization of the microporosity is obtained. In a 3D transmission electron tomogram the data is acquired from 2D projections at different tilt angles (in this case 120 projections) and combined, which makes it easier to visualize and interpret a large amount of data. It is possible to view the original sample from different angles or to cut the tomogram into thin "digital slices" to see the inside of the tomogram. The resolution $r$ of the reconstructed tomogram is dependent on the number of projections acquired $N$ and the thickness of the sample $d$, and can be estimated using the Crowther criterion $r = \pi^* d/N$.[56] In our case the sample thickness $d$ is ca. 50 nm and number of projections $N$ is 120, thus the estimated $r$ of the tomogram is ca. 1 nm. Figure 6a represents a 3D tomogram for the sample pyrolyzed at 420 °C for 60 min. A digital slice thickness of 1 nm of the randomly selected area of the tomogram is shown in Figure 6b. The thin slice illustrates the microporous structure within the phenolic matrix. The porosity is denser close to the mesopores, which is quite reasonable. We would like to point out that this result must be interpreted as preliminary, as we did not manage to produce related tomo-

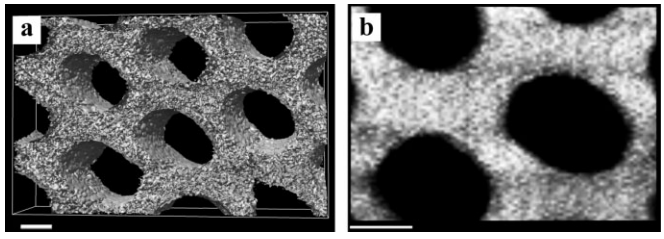


**Figure 6.** a) 3D tomogram of microtomed thin section of the sample isothermally pyrolyzed at 420 °C for 60 min, as rendered in isosurface mode showing surface roughness. b) 1 nm thick digital section of a selected area of the tomogram shown in figure (a) rendered in solid mode. The figure suggests micropores shown as black dots in the material. The scale bar in both images is 20 nm.

grams in a cured and non-pyrolyzed phenolic resin–P4VP-*b*-PS complex due to the lack of contrast in the sample. This may reflect the importance of the emptied mesoporous channels in a pyrolyzed phenolic resin–P4VP-*b*-PS complex for the channels to promote the removal of P4VP.

Previously we observed that the OH groups of the phenolic matrix remain after slowly heating up to 420 °C and that the porous structure and the hydroxyl groups of the phenolic matrix lead to a faster absorption rate and chemical selectivity towards hydrogen-bonding compounds.[29] To probe interactions at the pore walls, methylene blue (MB) hydrate dye is particularly useful, as there is a strong selective interaction due to the hydrogen bonding expected between the nitrogen-containing aromatic ring of MB and phenol. Absorption of MB solution in Milli-Q water (concentration less than 0.013 wt %) was investigated using UV-vis spectroscopy (Fig. 7). In order to study the absorption properties, hierarchical porous materials and phenolic-resin samples were immersed into the dye solution. In order to observe differences in the absorption properties between

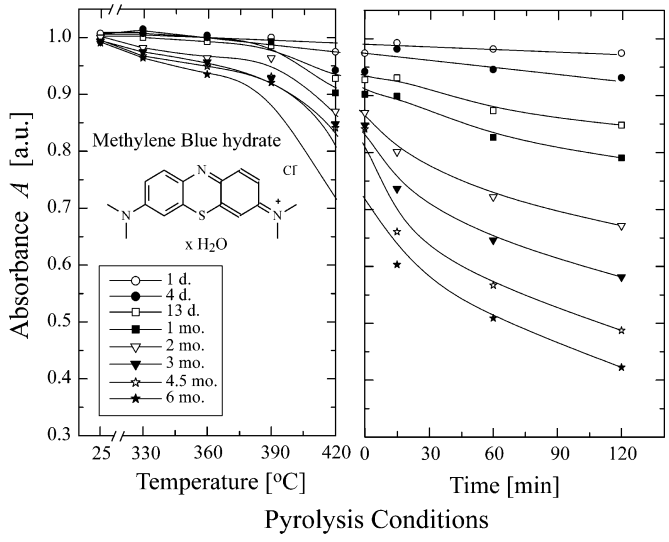


**Figure 7.** MB concentration in aqueous solutions as a function of time upon addition to (hierarchically) porous phenolic absorbents in the solutions. The concentration of MB is based on its characteristic UV-vis absorption at $\lambda = 665$ nm as a function of time. The *x*-axis separation is similar to what has been given in Figure 4. Note that the pure phenolic resin sample has been separated with a break in the *x*-axis.

the samples, the concentration of the MB molecules was selected to be relatively high. The characteristic UV-vis absorption maximum (at 665 nm for MB in water solution) at different times as a function of pyrolysis conditions is represented in Figure 7. The pure phenolic-resin sample and the sample slowly heated up to 330 °C absorb only a small amount of dye from the solution and no significant changes in absorption are observed. Also, for the samples slowly heated to 360, 390, and 420 °C absorption of MB from the solution is leveled off to a high absorbance level, indicating that a substantial amount of MB still remains in the solution. However, the samples with higher surface areas (isothermally pyrolyzed at 420 °C for 15, 60, and 120 min) absorb MB from solution more rapidly and the absorption does not level off even after six months. This clearly supports the expectation that the high absorption rate of MB results from the creation of hierarchical porosity.

## 3. Conclusions

We have shown a facile method to achieve self-assembled hierarchical porosity in polymers and to tune the porosity from mesoporous to hierarchically micro-mesoporous simply by controlling the pyrolysis conditions of cured block-copolymer–phenolic resin complexes. The mesoscale porosity results from the degraded PS block of P4VP-*b*-PS, whereas the microporosity is formed during the degradation of the P4VP block within the phenolic matrix. We expect that such materials could be useful for sensors, separation materials, filters, and templates for catalysis, as they have a high density of pores and a large surface area per volume unit as well as phenolic hydroxyl groups at the pore walls. Furthermore, these thermoset resin-based materials can be practically molded into any desired shape, not only as powders, which increases their range of applications significantly.

## 4. Experimental

*Materials*: P4VP-*b*-PS diblock copolymer ($M_{n,P4VP} = 5600$ g mol$^{-1}$, $M_{n,PS} = 40\,000$ g mol$^{-1}$, and $M_w/M_n = 1.09$) was provided by Polymer Source and was used without further purification. Phenolic resin (Novolac) was supplied by Bayer (Vulcadur RB). The crosslinking agent HMTA was acquired from Aldrich (99 + %) and tetrahydrofuran (THF) was provided by Riedel-de Haën (99.9 %).

*Sample Preparation*: In order to obtain a cylindrical structure, the weight percent of PS in the complexes was selected to be 40 % based on our previous results [29]. The Phenolic resin/HMTA ratio in all complexes was 88:12. Phenolic resin, HMTA, and P4VP-*b*-PS were dissolved in THF separately until the solutions were homogenous. The solutions were combined and the mixtures were stirred for one day at room temperature. THF was slowly evaporated at room temperature and thereafter the samples were vacuum dried at 30 °C for one day. Curing of the samples was performed using the following temperature profile: 100 °C for 2 h, 150 °C for 2 h, and finally 190 °C for 2 h. Pyrolysis of crosslinked samples was performed by slowly heating from room temperature up to 330–420 °C using a heating rate of 1 °C min$^{-1}$, without a protective gas atmosphere. Based on the TGA measurements, $T = 420$ °C was chosen to be the highest pyrolysis temperature, because at that temperature most of the block copolymer has been degraded whereas the weight of the cured phenolic matrix has not decreased significantly [29]. Therefore, instead of further heating, isothermal treatments of lengths of 0, 15, 30, 60, and 120 min were used at 420 °C.

*SAXS*: The SAXS measurements were performed at the Dutch–Belgian beamline (BM26B) of the European Synchrotron Radiation Facility in Grenoble, using a beam of 10 keV. The SAXS data were collected with a 2D multiwire proportional counter (MWPS) at a distance of 8.0 m from the sample. A description of the beamline is given elsewhere [57]. The magnitude of the scattering vector is given by $q = (4\pi/\lambda)\sin\theta$, where $2\theta$ is the scattering angle and $\lambda = 1.54$ Å.

*TEM and 3D-TEM*: The samples were embedded into epoxy Eponate 12, which was procured at 60 °C for 2 h in order to prevent the penetration of epoxy inside the pores. Final curing was performed at 60 °C for 20 h. Sections with a thickness of 40–70 nm were cut using

Leica Ultracut UCT ultramicrotome with a diamond knife and collected on 600 mesh-sized copper grids. Bright-field TEM was performed with a Tecnai 12 transmission electron microscope using a 120 kV accelerating voltage. Data for 3D-TEM was collected automatically using UCSF Tomography software [58] and a Gatan UltraScan 1000 camera with a charge-coupled device (CCD) size of $2048 \times 2048$. The acquired image stack covered the angular range of ±60° with one degree steps, at a magnification of 68 000. Gold ficiduals with a diameter of 15 nm were used for image alignment. Tomograms were reconstructed with a maximum entropy method using a custom software package [59]. In addition UCSF Chimera software was used for tomogram visualization [60]. The resolution $r$ of the reconstructed tomogram is dependent on the number of projections acquired $N$ and the thickness of the sample $d$ and can be estimated by the Crowther criterion $r = \pi^* d/N$ [56]. However, the resolution in the direction parallel to the optical axis is less than the spatial resolution because of the "missing wedge" on the tilt range [61]. The microporous structure within the phenolic matrix is expected to be disordered and thus the decrease in resolution in one direction should not prevent the observation of the micropores in a thin slice of the tomogram. To further improve the accuracy, images were oversampled by acquiring micrographs at a sufficiently large magnification of 68 000, which resulted in a pixel size of 0.168 nm. To compensate for oversampling, the original images were binned six times during the tomogram reconstruction, which leads to the actual pixel size of ca. 1 nm in the tomograms. This coincides with the Crowther criterion.

*PALS*: PALS measurements were performed with a conventional fast–fast coincidence timing spectrometer with a time resolution of 0.270 ns (full width at half maximum) determined from a $^{60}$Co prompt spectrum. A $^{22}$Na positron source with an activity of 8 μCi was deposited and sealed between two thin aluminum foils. Two films (thickness: ca. 400 μm and lateral dimensions: 8 mm × 8 mm) of cured phenolic resin–P4VP-*b*-PS samples were stacked on either side of the source to form source sample sandwich geometry. This was placed between two scintillation detectors for positron lifetime measurements. A positron lifetime spectrum with more than one million counts was accumulated at each level of pyrolysis and the average values from ten measurements are reported. In this method, the survival time of positrons in a medium is measured. When an energetic positron from a radioactive source (commonly $^{22}$Na) enters a medium, it thermalizes in a very short time after interacting with the surrounding molecules through inelastic collisions. The o-Ps lifetime ($\tau_3$), along with the corresponding lifetime intensity ($I_3$), which is proportional to the fraction of o-Ps annihilations, are used to estimate the mean size and often also the relative density of free-volume holes in a polymer sample [47, 48, 62]. The PALS spectra of a cured but not pyrolyzed reference sample phenolic resin–P4VP-*b*-PS and those at different conditions of pyrolysis are analyzed using the program PATFIT-88 [63]. The results of the four-component analysis are not as reliable as the three-component fit as the former results are with large standard deviations. Hence, we interpret the results in terms of three-lifetime components. The three-lifetime component analysis results have been previously reported for novolac epoxy resins [48, 64]. Since only the long-lived o-Ps lifetime ($\tau_3$) and its intensity ($I_3$) could be related to the properties of the pores in the samples the discussions are based on the annihilation characteristics of the third component.

*Surface-Area Measurement*: The surface area and porosity measurements were performed with a Coulter Omnisorp 100CX gas adsorption instrument using static volumetric adsorption and desorption method. After loading the sample it was first evacuated at room temperature to a pressure of $1 \times 10^{-4}$ Torr (1 Torr = 133.322 Pa) or lower. Then, the evacuating temperature was raised first to 90 °C where the sample was evacuated for at least half an hour and thereafter the temperature was raised to a final evacuation temperature of 200 °C. Evacuation at the final temperature was continued until the pressure went below $1 \times 10^{-5}$ Torr; a typical evacuation time at the final temperature was between 3 and 4 h. Nitrogen was used as an adsorptive gas and measurements were done at a liquid-nitrogen bath at 77 K. Adsorption isotherm were measured by dosing nitrogen to the sample and measuring the adsorbed amount as a function of nitrogen pressure.

*UV-vis Spectroscopy*: Absorption properties of the pyrolyzed phenolic materials were studied as a function of time using MB hydrate (Fluka 97 %) dissolved in Milli-Q water. The specular UV-vis spectra were measured using a Perkin–Elmer Lambda 950 spectrophotometer in the wavelength range 250–900 nm. The samples for UV-vis measurements were prepared as follows: First, MB was dissolved in water at a concentration less than 0.013 wt %. Thereafter, the hierarchical porous materials (with different pyrolysis conditions) and reference samples (pure phenolic resin and cured but not pyrolyzed phenolic resin–P4VP-*b*-PS) were immersed into the solutions (samples were ground using a mortar). The amount of the materials was selected so that the number of MB molecules was 6.25 % of the nominal moles of the hydroxyl groups of the phenolic resin.

Received: July 7, 2006
Revised: August 1, 2006
Published online: December 19, 2006

[1] M. Hartmann, *Angew. Chem. Int. Ed.* **2004**, *43*, 5880.
[2] C. F. Blanford, H. Yan, R. C. Schroden, M. Al-Daous, A. Stein, *Adv. Mater.* **2001**, *13*, 401.
[3] X. S. Zhao, *J. Mater. Chem.* **2006**, *16*, 623.
[4] Z.-Y. Yuan, B.-L. Su, *J. Mater. Chem.* **2006**, *16*, 663.
[5] S. Polarz, M. Antonietti, *Chem. Commun.* **2002**, 2593.
[6] C. J. Brinker, *Curr. Opin. Solid State Mater. Sci.* **1996**, *1*, 798.
[7] G. J. de Soler-Illia, C. Sanchez, B. Lebeau, J. Patarin, *Chem. Rev.* **2002**, *102*, 4093.
[8] T. O. Drews, M. Tsapatsis, *Curr. Opin. Colloid Interface Sci.* **2005**, *10*, 233.
[9] P. F. W. Simon, R. Ulrich, H. W. Spiess, U. Wiesner, *Chem. Mater.* **2001**, *13*, 3464.
[10] T. Hayakawa, S. Horiuchi, *Angew. Chem. Int. Ed.* **2003**, *42*, 2285.
[11] Y. Zhou, M. Antonietti, *Chem. Commun.* **2003**, 2564.
[12] C.-M. Yang, B. Zibrowius, W. Schmidt, F. Schüth, *Chem. Mater.* **2003**, *15*, 3739.
[13] H. Maekawa, J. Esquena, S. Bishop, C. Solans, B. F. Chmelka, *Adv. Mater.* **2003**, *15*, 591.
[14] M. Antonietti, B. Berton, C. Göltner, H.-P. Hentze, *Adv. Mater.* **1998**, *10*, 154.
[15] O. Sel, D. Kuang, M. Thommes, B. Smarsly, *Langmuir* **2006**, *22*, 2311.
[16] S. Mann, S. L. Burkett, S. A. Davis, C. E. Fowler, N. H. Mendelson, S. D. Sims, D. Walsh, N. T. Whilton, *Chem. Mater.* **1997**, *9*, 2300.
[17] J.-H. Sun, Z. Shan, T. Maschmayer, M.-O. Coppens, *Langmuir* **2003**, *19*, 8395.
[18] A. Okabe, M. Niki, T. Fukushima, T. Aida, *J. Mater. Chem.* **2005**, *15*, 1329.
[19] D. Kuang, T. Brezesinski, B. Smarsly, *J. Am. Chem. Soc.* **2004**, *126*, 10 534.
[20] T. Sen, G. J. T. Tiddy, J. L. Casci, M. W. Anderson, *Angew. Chem. Int. Ed.* **2003**, *42*, 4649.
[21] D. Brandhuber, N. Huesing, C. K. Raab, V. Torma, H. Peterlik, *J. Mater. Chem.* **2005**, *15*, 1801.
[22] X. S. Zhao, F. Su, Q. Yan, W. Guo, X. Y. Bao, L. Lv, Z. Zhou, *J. Mater. Chem.* **2006**, *16*, 637.
[23] H.-P. Hentze, M. Antonietti, *Curr. Opin. Solid State Mater. Sci.* **2001**, *6*, 343.
[24] A. Taguchi, J.-H. Smatt, M. Linden, *Adv. Mater.* **2003**, *15*, 1209.
[25] Q. Huo, D. Margolese, U. Ciesla, P. Feng, T. E. Gier, P. Sieger, R. Leon, P. M. Petroff, F. Schüth, G. D. Stucky, *Nature* **1994**, *368*, 317.
[26] C. T. Kresge, M. E. Leonowicz, W. J. Roth, J. C. Vartuli, J. S. Beck, *Nature* **1992**, *359*, 710.
[27] A. Monnier, F. Schüth, Q. Huo, D. Kumar, D. Margolese, R. S. Maxwell, G. D. Stucky, M. Krishamurty, P. Petroff, A. Firouzi, M. Janicke, B. F. Chmelka, *Science* **1993**, *261*, 1299.
[28] T. Thurn-Albrecht, J. Schotter, G. A. Kästle, N. Emley, T. Shibauchi, L. Krusin-Elbaum, K. Guarini, C. T. Black, M. T. Tuominen, T. P. Russell, *Science* **2000**, *290*, 2126.

[29] H. Kosonen, S. Valkama, A. Nykänen, M. Toivanen, G. ten Brinke, J. Ruokolainen, O. Ikkala, *Adv. Mater.* **2006**, *18*, 201.
[30] C. Liang, S. Dai, *J. Am. Chem. Soc.* **2006**, *128*, 5316.
[31] C. Liang, K. Hong, G. A. Guiochon, J. W. Mays, S. Dai, *Angew. Chem. Int. Ed.* **2004**, *43*, 5785.
[32] B. T. Holland, C. F. Blanford, A. Stein, *Science* **1998**, *281*, 538.
[33] O. D. Velev, T. A. Jede, R. F. Lobo, A. M. Lenhoff, *Nature* **1997**, *389*, 447.
[34] A. Imhof, D. J. Pine, *Nature* **1997**, *389*, 948.
[35] M. Breulmann, S. A. Davis, S. Mann, H.-P. Hentze, M. Antonietti, *Adv. Mater.* **2000**, *12*, 502.
[36] D. M. Antonelli, *Microporous Mesoporous Mater.* **1999**, *33*, 209.
[37] P. Sepulveda, J. G. P. Binner, *J. Eur. Ceram. Soc.* **1999**, *19*, 2059.
[38] S. A. Davis, S. L. Burkett, N. H. Mendelson, S. Mann, *Nature* **1997**, *385*, 420.
[39] F. S. Bates, G. H. Fredrickson, *Annu. Rev. Phys. Chem.* **1990**, *41*, 525.
[40] H. Kosonen, J. Ruokolainen, P. Nyholm, O. Ikkala, *Macromolecules* **2001**, *34*, 3046.
[41] H. Kosonen, J. Ruokolainen, M. Torkkeli, R. Serimaa, P. Nyholm, O. Ikkala, *Macromol. Chem. Phys.* **2002**, *293*, 388.
[42] Y.-J. Lee, J. S. Lee, Y. S. Park, K. B. Yoon, *Adv. Mater.* **2001**, *13*, 1259.
[43] K. Nakanishi, *J. Porous Mater.* **1997**, *4*, 67.
[44] T. C. Merkel, B. D. Freeman, R. J. Spontak, Z. He, I. Pinnau, P. Meakin, A. J. Hill, *Science* **2002**, *296*, 519.
[45] O. E. Mogensen, *Positron Annihilation in Chemistry*, Springer, Berlin **1995**.
[46] R. Stephen, C. Ranganathaiah, S. Varghese, K. Joseph, S. Thomas, *Polymer* **2006**, *47*, 858.
[47] J. M. G. Cowie, I. McEwan, I. J. McEwen, R. A. Pethrick, *Macromolecules* **2001**, *34*, 7071.
[48] Y. C. Jean, *Microchem. J.* **1990**, *42*, 72.
[49] T. Goworek, *Radiat. Phys. Chem.* **2003**, *68*, 331.
[50] T. Mincov, M. P. Petkov, P. Tsou, T. Troev, *J. Non-Cryst. Solids* **2004**, *350*, 253.
[51] G. P. Babu, V. Manohar, K. Sudarshan, P. K. Pujari, S. B. Manohar, A. Goswami, *J. Phys. Chem. B* **2002**, *106*, 6902.
[52] K. Venkateswaran, K. L. Cheng, Y. C. Jean, *J. Phys. Chem.* **1984**, *88*, 2465.
[53] S. J. Tao, *J. Chem. Phys.* **1972**, *56*, 5499.
[54] M. Eldrup, D. Lightbody, J. Sherwood, *Chem. Phys.* **1981**, *63*, 51.
[55] H. Nakanishi, S. J. Wang, Y. C. Jean, *Positron Annihilation Studies of Fluids*, World Scientific, Singapore **1988**.
[56] R. A. Crowther, D. J. DeRosier, A. Klug, *Proc. R. Soc. London Ser. A* **1970**, *317*, 319.
[57] W. Bras, *J. Macromol. Sci., Part B, Phys.* **1998**, *37*, 557.
[58] Q. S. Zheng, M. B. Braunfeld, J. W. Sedat, D. A. Agard, *J. Struct. Biol.* **2004**, *147*, 91.
[59] P. Engelhardt, in *Encyclopedia of Analytical Chemistry*, Vol. 6 (Ed: R. A. Mayers) Wiley, Chichester, UK **2000**, p. 4948.
[60] E. F. Pettersen, T. D. Goddard, C. C. Huang, G. S. Couch, D. M. Greenblatt, E. C. Meng, T. E. Ferrin, *J. Comput. Chem.* **2004**, *25*, 1605.
[61] V. Lucic, F. Forster, W. Baumeister, *Annu. Rev. Biochem.* **2005**, *74*, 833.
[62] *Principles and Application of Positron and Positronium Chemistry* (Eds: Y. C. Jean, P. E. Mallon, D. M. Schrader), World Scientific, Singapore **2003**.
[63] P. Kirkegaard, N. J. Pedersen, M. Eldrup, *Riso National Laboratory Report M-2740*, Denmark **1989**.
[64] T. Suzuki, Y. Oki, M. Numajiri, T. Miura, K. Kondo, Y. Shiomi, Y. Ito, *Polymer* **1996**, *37*, 3025.